

## Discussion on ultimate resistance formulas of high-strength bolts under tensile-shear coupling loading

Xin, Haohui; Liu, Gao; Zhang, Youyou; Guo, Xiao; Li, Jie; Veljkovic, Milan

**DOI**

[10.1016/j.jcsr.2024.108848](https://doi.org/10.1016/j.jcsr.2024.108848)

**Publication date**

2024

**Document Version**

Final published version

**Published in**

Journal of Constructional Steel Research

**Citation (APA)**

Xin, H., Liu, G., Zhang, Y., Guo, X., Li, J., & Veljkovic, M. (2024). Discussion on ultimate resistance formulas of high-strength bolts under tensile-shear coupling loading. *Journal of Constructional Steel Research*, 220, Article 108848. <https://doi.org/10.1016/j.jcsr.2024.108848>

**Important note**

To cite this publication, please use the final published version (if applicable). Please check the document version above.

**Copyright**

Other than for strictly personal use, it is not permitted to download, forward or distribute the text or part of it, without the consent of the author(s) and/or copyright holder(s), unless the work is under an open content license such as Creative Commons.

**Takedown policy**

Please contact us and provide details if you believe this document breaches copyrights. We will remove access to the work immediately and investigate your claim.

***Green Open Access added to TU Delft Institutional Repository***

***'You share, we take care!' - Taverne project***

**<https://www.openaccess.nl/en/you-share-we-take-care>**

Otherwise as indicated in the copyright section: the publisher is the copyright holder of this work and the author uses the Dutch legislation to make this work public.



## Discussion on ultimate resistance formulas of high-strength bolts under tensile-shear coupling loading

Haohui Xin<sup>a,b</sup>, Gao Liu<sup>a,b</sup>, Youyou Zhang<sup>c,\*</sup>, Xiao Guo<sup>d,e</sup>, Jie Li<sup>c</sup>, Milan Veljkovic<sup>f</sup>

<sup>a</sup> School of Civil Engineering, Southeast University, Nanjing 211189, China

<sup>b</sup> State Key Laboratory of Safety, Durability and Healthy Operation of Long Span Bridges, Nanjing 211189, China

<sup>c</sup> Department of Civil Engineering, Xi'an Jiaotong University, Xi'an 710116, China

<sup>d</sup> Guangxi Key Laboratory of Disaster Prevention and Engineering Safety, Guangxi University, Nanjing 530004, China

<sup>e</sup> College of Civil engineering and Architecture, Guangxi University, Nanjing 530004, China

<sup>f</sup> Faculty of Civil Engineering and Geosciences, Delft University of Technology, Delft 2600AA, the Netherlands

### ARTICLE INFO

#### Keywords:

High-strength bolts  
Ultimate resistance  
Influencing factors  
Numerical simulation  
Design specifications

### ABSTRACT

Bolted connections are one of the key connection configurations in steel structures. The ductile fracture prediction is one of the challenges in the structural integrity evaluating of steel structures. To guarantee the safety of steel bridge in connections, an accurate assessment of the ultimate resistance of high-strength bolts under combined tensile-shear loads is necessary. However, the impacts of various parameters on high-strength bolts under combined tensile-shear loads are not sufficiently analysed in the existing references. Hence, in this paper, the validated mesoscale critical equivalent plastic strain (MCEPS) method is used to evaluate the ultimate resistance of high-strength bolts with different bolt grades, bolt diameters, bolt types, hole clearance, and preload force when the bolts are exposed to combined tensile-shear loading. The simulation results are compared to existing design specifications. Finally, the formula modifications in the existing design standards are proposed based on statistical analysis on numerical parametric results.

### 1. Introduction

When evaluating the structural integrity of steel constructions, connections are frequently the most important factor. Bolts, one of the most fundamental forms of connections, are used to convey external force between two components. Properly designed bolted connections should not be the weak link caused by the lower ductility during load transferring [1,2]. Any damage to the bolted connections will compromise the structural integrity of the entire structure, and structural failure may eventually occur. [3]. Ductile fracture of steel connectors under occasional extreme loading is therefore one of the challenges in assessing the structural integrity of connections during steel structures design [4].

The failure of bolted connections could be divided into two types: steel plates and high strength bolts. To ensure the safety of bolted connections, i.e. the safety of the entire steel bridge structure, the ultimate resistance of high strength bolts under composite loads must be accurately assessed, in addition to steel plates. Current steel design standards propose equations for assessing the ultimate strength of high strength

bolts, including the GB-50017 [5] in China, the EN 1993-1-8 (EC3) in Europe [6], the AISC-360 in the USA [7], and the AS 4100 in Australia [8]. Noted that the grade of the high-strength bolt is limited to Grade 8.8 in AS 4100, Grade 10.9 in EC3, GB-50017, and AISC-360. Use of Grade 12.9 bolts in steel constructions is restricted by the lack of adequate experimental findings and design formulas. The prediction formula for high-strength bolts exposed to combined tensile-shear loading shows scattering from the existing design formulas. It means that the influence of various parameters was not clearly addressed in the reduction of bearing resistance.

Several researchers have used experimental or numerical methods to predict the maximum resistance of bolts [9–14]. However, the bolt serves as a connection within the joint regions to guarantee the consistency of the load transmission, and it must withstand multiple events at once, especially in a coupled tensile-shear condition. Only a small amount of research has considered the complex load effects in earlier literature [15–19]. Influence of various parameters on the bearing resistance of high-strength bolts under complex stress states (combines tension and shear loading) requires rather cumbersome test-setup [20,21]. In addition, establishing all pertinent bolted connection

\* Corresponding author.

E-mail address: [youyouzhang@xjtu.edu.cn](mailto:youyouzhang@xjtu.edu.cn) (Y. Zhang).

<https://doi.org/10.1016/j.jcsr.2024.108848>

Received 23 August 2023; Received in revised form 8 June 2024; Accepted 15 June 2024

Available online 26 June 2024

0143-974X/© 2024 Elsevier Ltd. All rights reserved, including those for text and data mining, AI training, and similar technologies.

**Nomenclature**

$A, A_s$  gross, equivalent cross-section area of the bolt in EC3.  
 $A_c, A_0$  area with minor diameter/nominal plain-shank of the bolt in AS 4100.  
 $C, C_1, C_2, C_3$  the cut-off value/the calibrated parameter in ductile fracture locus eq.  $C = 1/3$   
 $C'$  constant coefficient in the modified equation.  
 $F_{nt}, F_{nt}', F_{nv}, F_{nv}'$  nominal tensile/shear strength in AISC-360.  
 $\bar{L}$  Lode parameter averaged over the loading history.  
 $N_f$  nominal tensile capacity of a bolt in AS 4100.  
 $P_y, P_x, P_u$  ultimate resistance in the tensile direction, shear direction, and combined direction.  
 $P_0$  the theoretical ultimate tensile strength resistance of high-strength bolts; defined as  $P_0 = f_u^b A_s$ .  
 $U_y, U_x$  axial/shear displacement.  
 $V_f$  nominal shear capacity of a bolt in AS 4100.  
 $f_u^b, f_t^b, f_v^b$  the ultimate/equivalent tensile/shear strength for the tensile resistance prediction.  
 $f_{rv}, f_{rt}$  required shear/tensile stress using LRFD or ASD load combinations in AISC-360.

$f_{uf}$  minimum tensile strength of the bolt in AS 4100.  
 $k$  loading factor for shear resistance in the modified equation.  
 $k_2$  reduction factor in Eurocode 3,  $k_2 = 0.9$ .  
 $k_r$  reduction factor to account for the length of a bolted lap connection; defined as 1.0.  
 $m$  power coefficient in modified equation.  
 $n_n, n_x$  number of shear planes with/without threads intercepting the shear plane.  
 $\alpha_v$  reduction factor for shear resistance in Eurocode 3;  
 $\bar{\epsilon}^p, \bar{\epsilon}_u^p, \bar{\epsilon}_{pl,f}^p$  corresponding/maximum/fracture plastic strain when the true stress without considering necking and damage effects.  
 $\bar{\eta}$  stress triaxiality averaged over the loading history.  
 $\Phi$  capacity factor in AS 4100; defined as 0.8.  
 $\gamma_t, \gamma_v$  limit in the tensile/shear direction in the modified equation.  
 $\gamma_{M2}$  partial safety factor of ultimate resistance in Eurocode 3.  
 $\delta_y, \delta_x$  fracture deformation in axial tension/shear direction.  
 $\xi_t, \xi_v$  multiaxial loading factor for tensile/shear resistance.  
 $\bar{\sigma}^{neck}, \bar{\sigma}$  corrected true stress for necking and post-damage.

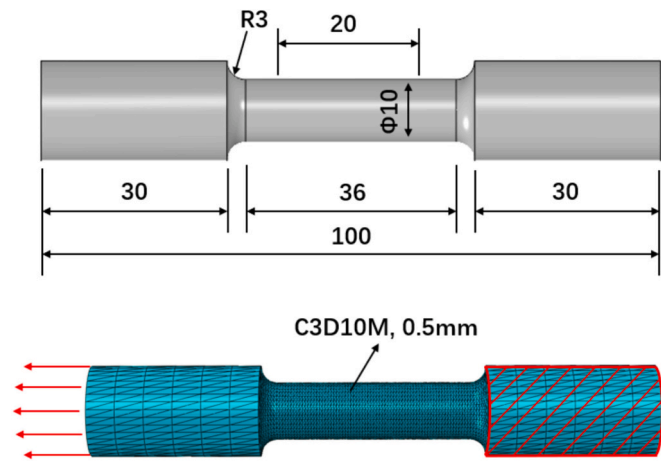


Fig. 1. Geometric size and Boundary condition of the Tension specimen (Units: mm).

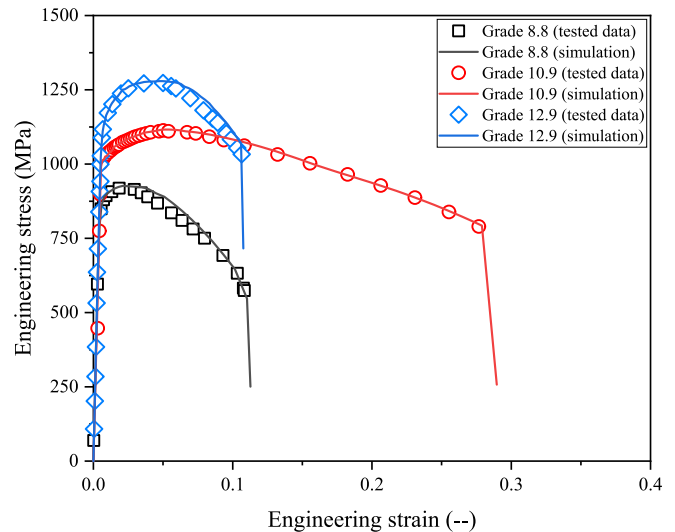


Fig. 2. Engineering stress-strain of high strength bolts.

configurations takes a lot of time and money for full-scale trials. A solution is provided by finite element simulation (FE), which accurately captures the mechanical properties of high-strength bolts and predicts their eventual bearing performance under challenging situations [22–26].

In this paper, the uncoupled ductile fracture model of high-strength steel was adopted to analyse the failure of high-strength bolts under different influencing factors using the mesoscale failure index [27–29]. Experimental results were obtained from reference [19, 30], and a good agreement was obtained by comparing with the experimental results. Afterward, five interesting parameters, including steel grade, type (partially or fully threaded), diameter, hole clearance, and pretension force, were considered as the influencing factor for numerical simulation. Furthermore, the simulated results were compared with the existing international design provisions, and modifications were proposed to the design standards to improve the accuracy of predictions.

**2. Validation of finite element model**

**2.1. Stress-strain relationship**

The FE software ABAQUS was used to predict the ductile fracture of bolts. The material parameters of the uncoupled ductile fracture model were calibrated using mesoscale critical equivalent plastic strain (MCEPS) methods. The material parameters calibration of the uncoupled ductile fracture model could be divided into two parts. First part, calibrating material parameters for true stress-strain curves with emphasis on post-necking stage by comparing numerical results and experimental data. More detailed procedures can be referred to [27]. Second part, calibrating the fracture locus using mesoscale critical equivalent plastic strain (MCEPS) as failure index based on computational homogenization methods. More detailed procedures can be referred to [28,29]. The explanations of material parameters were described in Appendix A. The tensile specimen was conducted under

**Table 1**  
Calibrated material parameter of high strength bolts (mesh size = 0.5 mm).\*

Grade	8.8	10.9	12.9
Elastic Modulus E (GPa)	202.95	207.08	200.69
Yield Strength (MPa)	857.38	1003.82	1125.63
Ultimate Strength (MPa)	924.97	1175.46	1281.31
W	0	0	0
$\bar{\sigma}_u$	943.94	1247.15	1336.41
$\bar{\epsilon}_u^p$	0.0203	0.0592	0.0421
$\bar{\epsilon}_{d-i}^p$	0.0489	0.0839	0.0532
C <sub>1</sub>	2.64	2.70	1.86
C <sub>2</sub>	0.78	0.31	0.57
C <sub>3</sub>	0.83	0.66	0.46

\* Note: C<sub>1</sub>, C<sub>2</sub>, C<sub>3</sub> are material parameters of fracture locus, the detailed equations are shown in Appendix A.

displacement control mode, as presented in Fig. 1. The C3D10M triangular elements were used with the fixed size of 0.5 mm. The time increment was set to  $1 \times 10^{-5}$  s. The ductile fracture simulation was achieved via the VUSDFLD user subroutine. Fig. 2 shows the results of the parametric calibration of high strength bolts of grades 8.8, 10.9, and 12.9 with a mesh size of 0.5 mm. Noted that the mesh size will affect the fracture parameters in Table 1 [31]. A good agreement was observed when comparing the stress-strain relationships of the calibrated results

with the tested data. The difference of ultimate strengths and engineering strain at fracture point was within 5%, which can be considered as a high fidelity for the material parameter calibration.

The boundary conditions and geometry of the combined tensile-shear bearing model are shown in Fig. 3. The bolt was loaded by two blocks with linear elastic material properties, considered all contact surfaces set to ‘hard contact’ in normal direction and a coefficient of friction of 0.3 in the tangential direction. The elastic modulus is defined as 210.0GPa and the Possion’s ratio is defined as 0.3 for the steel loading block. Two reference points RP-1 and RP-2 were assigned to the upper and lower blocks. The different ratios of axial and tangential displacement were applied to the RP-1, whilst the RP-2 was fixed. The dimensions of the bolt, nut, and pitch were important for the simulation of

**Table 2**  
Geometry dimensions of high strength bolts.

Geometry size	Nut (mm)		Bolt (mm)		
	Diameter	Thickness	Pitch	Diameter	
				D <sub>maj</sub>	D <sub>p</sub>
M16	27	14	2.0	16	14.72
M20	34	17	2.5	20	18.38
M24	36	21	3.0	24	22.05

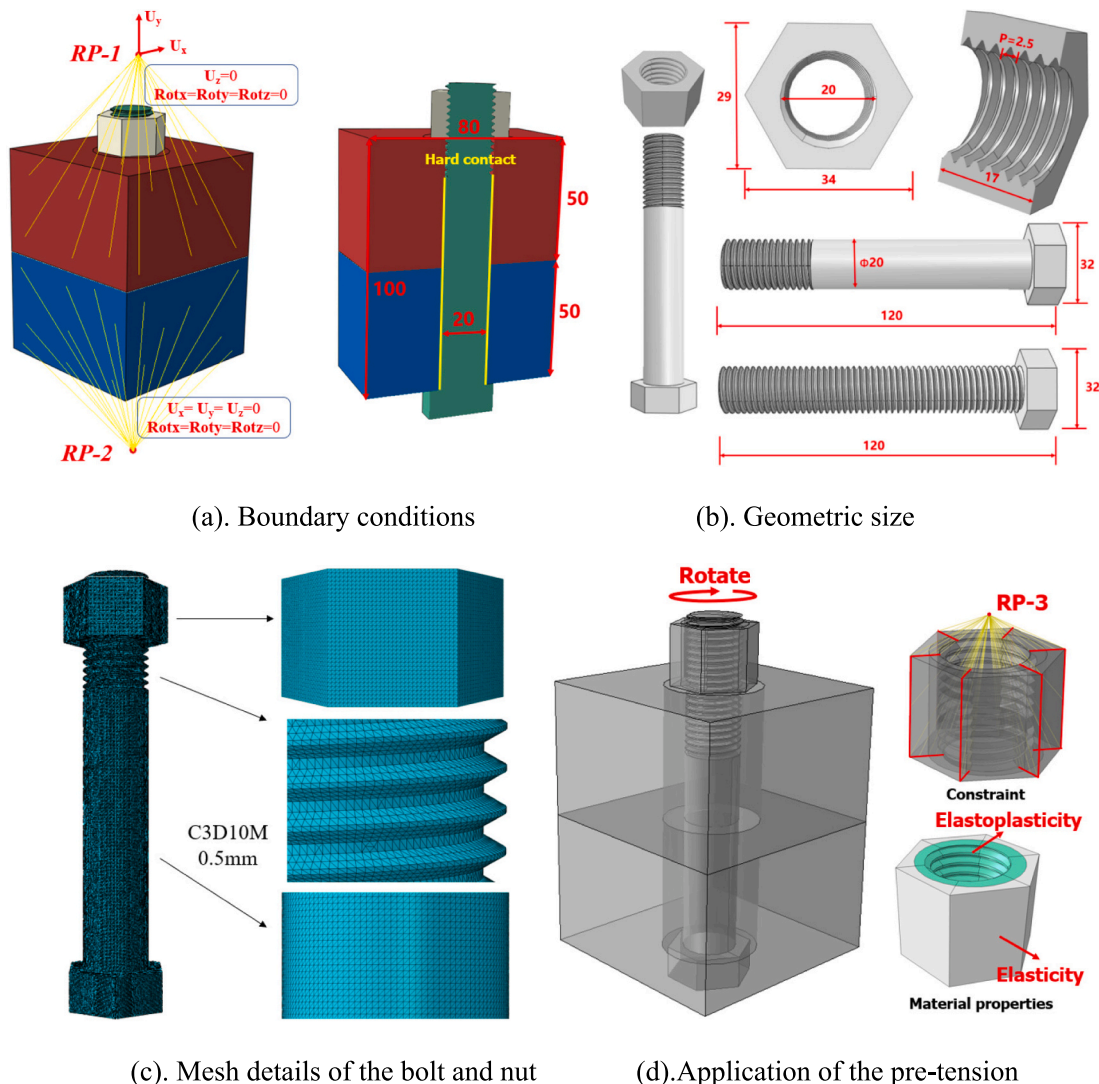


Fig. 3. Boundary condition and geometric size of the model.

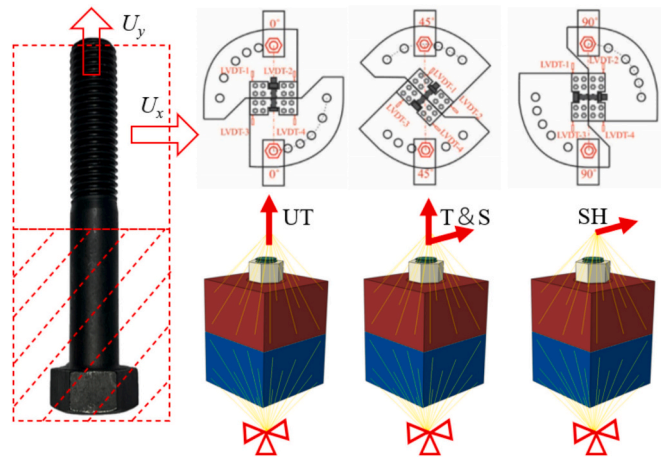


Fig. 4. Loading conditions for validated model.

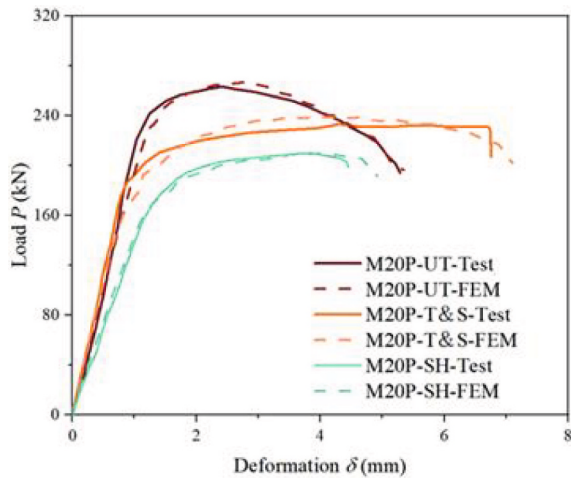
the components, which were specified in accordance with specifications IS 262:2:1998 [32] and EN 14399-3 [33] respectively. The detailed dimensions are summarized in Table 2. The reference point RP-3 was

coupled with each edge of the nut when pre-tension force was required by turning the nut. To prevent excessive deformation of the nut during the turning process, the nut was divided into two parts, with an elastoplastic material on the inside and an elastic material on the outside, as shown in Fig. 3(d).

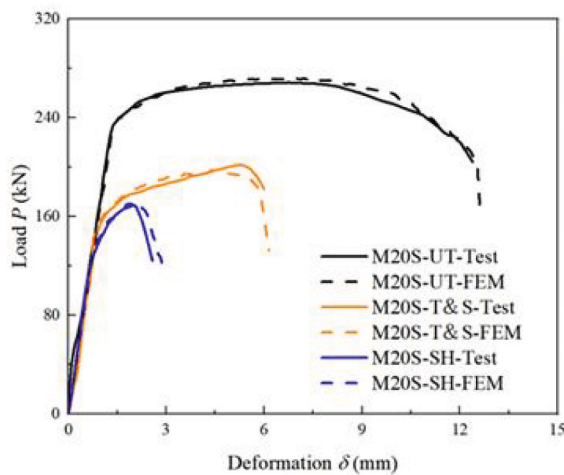
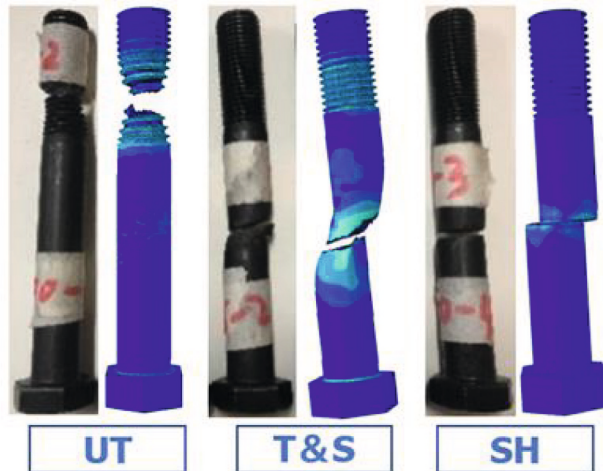
### 2.2. Comparisons between FE simulation and test results

The strength and deformation capacity of M20 bolts with Grade 10.9 under different loading combinations were utilized to validate the developed numerical model, three loading conditions (uniaxial tension loading, equal combined tensile and shear loading, pure shear loading) were selected for comparison, as shown in Fig. 4. The bolt deformation was calculated from the square root of the component deformation in both directions and the load was obtained by extracting the resistance of the block.

Fig. 5 compared the deformation-load relationship of the bolt between FE simulation and test results, showing a 2.4% difference in ultimate resistance for partially threaded bolt of grade 10.9, 2.3% for fully threaded bolt of grade 10.9. Furthermore, the fracture pattern of the bolt in the FE simulation showed a good agreement with the test observations. The ductile fractures of high strength bolt were successfully assessed using the suggested FE model, which also showed consistency



(a). Partially threaded bolt of Grade 10.9 (Test data from Ref[30])



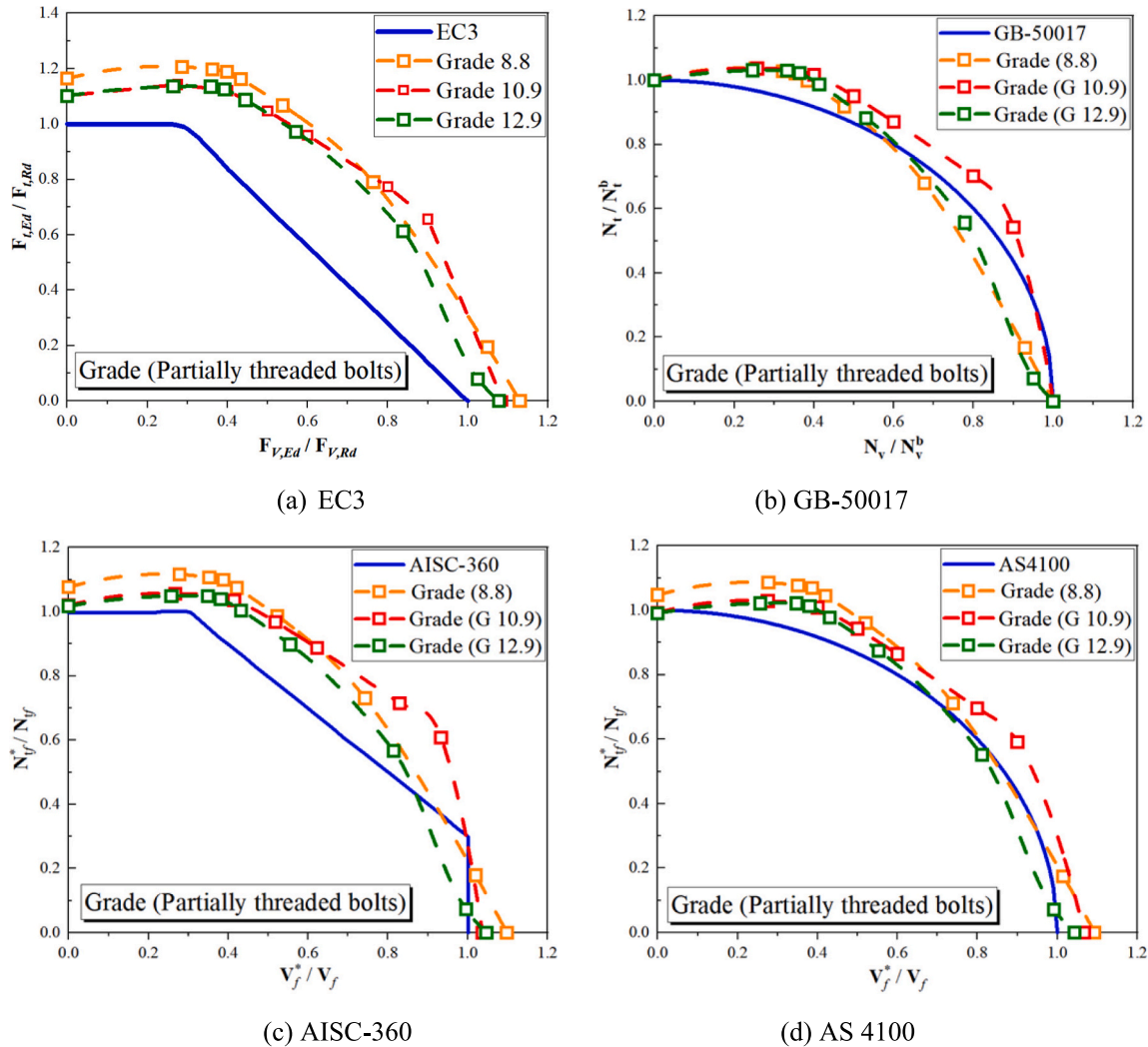
(b). Fully threaded bolt of Grade 10.9 (Test data from Ref [30])



Fig. 5. Comparisons of the simulated and tested results.

**Table 3**  
Ultimate capacity for various grades of High-strength bolts at different loading modes.

Bolt		Tensile-shear displacement ratio ( $U_y/U_x$ )								
		$\infty$ (UT)	5	2	1.25	1	0.8	0.5	0.2	0 (SH)
G8.8 (kN)	$P_y$	250.141	259.265	257.232	255.428	249.586	229.267	169.672	41.597	0
	$P_x$	0	48.576	61.587	67.718	73.559	91.226	129.650	177.954	191.656
	$P_u$	250.141	263.776	264.502	264.252	260.200	246.750	213.536	182.751	191.656
G10.9 (kN)	$P_y$	315.922	327.426	326.989	316.029	300.956	276.346	188.183	29.790	0
	$P_x$	0	62.368	96.177	103.305	120.774	151.245	189.823	233.244	241.361
	$P_u$	315.922	333.313	340.840	332.485	324.285	315.027	267.293	235.139	241.361
G12.9 (kN)	$P_y$	341.806	352.293	352.181	349.210	337.245	301.437	190.143	24.518	0
	$P_x$	0	64.959	87.989	96.233	109.094	140.052	205.438	251.078	264.008
	$P_u$	341.806	358.232	363.006	362.227	354.451	332.383	279.927	252.272	264.008



**Fig. 6.** Ultimate resistance comparisons with different steel grades.

in fracture deformation, failure mode, and ultimate resistance.

### 3. Parametric analysis

This study attempted to reveal the ultimate resistance behaviour of high strength bolts through a series of parametric studies using the validated numerical model. Five practical parameters of bolt, including grade, type, diameter, hole tolerance, and preload force, were considered, and the ultimate resistance was extracted in different combinations of tension and shear loading. The simulation results obtained were further compared with assessment equations in the relevant

specifications. The bolt-related calculation formular are in [Appendix B](#).

#### 3.1. Effects of bolt grade

For partially threaded bolts with a diameter of 20 mm, zero-hole clearance but without preload force, the ultimate resistance was predicted in terms of different steel grades, including Grade 8.8, Grade 10.9, and Grade 12.9 respectively. [Table 3](#) and [Fig. 6](#) compared the ultimate resistance of bolts with different grades between theoretical values in four design codes and FE predicted results. Under combined tensile-shear loading, higher grade high-strength bolts exhibit lower

**Table 4**  
Simulated result of M16 bolt ultimate capacity.

Simulated grade 10.9 bolts		Tensile-shear displacement ratio ( $D_y/D_x$ )							
		$\infty$ (UT)	3.73	1.73	1	0.58	0.27	0 (SH)	
M16P	$P_y$	214.503	218.218	216.548	206.844	173.214	128.448	0	
	$P_x$	0	29.142	55.741	65.289	97.933	130.578	163.223	
	$P_u$	214.503	220.156	223.607	216.903	198.982	183.166	163.223	
M16S	$P_y$	190.227	188.102	180.960	165.709	147.983	124.148	0	
	$P_x$	0	20.366	40.732	61.098	81.464	101.830	122.822	
	$P_u$	190.227	189.201	185.488	176.614	168.924	160.568	122.822	
$P_0$ (kN)			203.660						

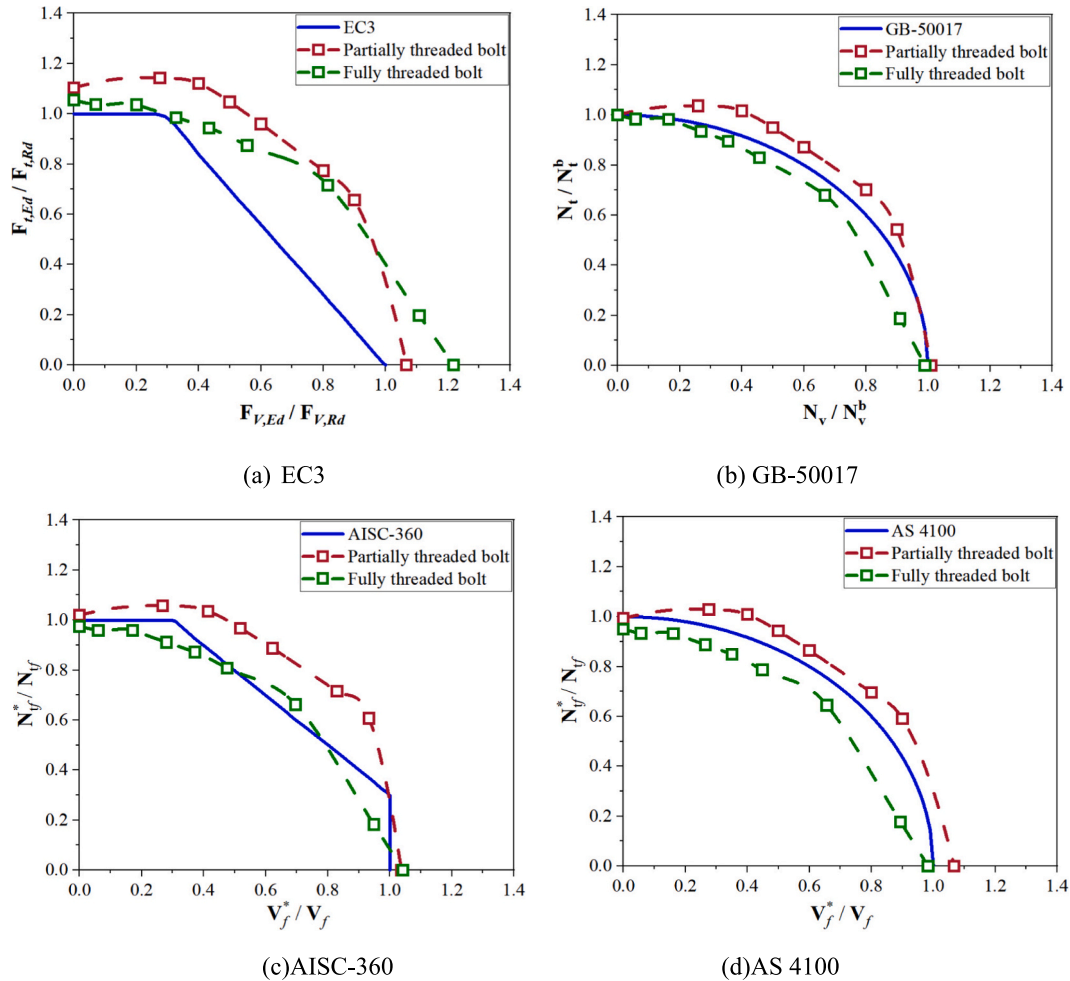


**Fig. 7.** Ultimate resistance comparisons with different bolt type.

normalized strength and performance lower plastic deformation capacity, making them more prone to fracture.

In terms of EC3 formulas, the ultimate resistance was slightly increased when a modest amount of shear force is applied, that is  $0 < F_{V,Ed}/F_{V,Rd} < 0.40$ ; but the ultimate resistance decreased monotonically with increasing contribution of the shear force, that is  $0.4 < F_{V,Ed}/F_{V,Rd} < 1.0$ . The predicted results are conservative for almost all cases. The envelope curve of grade 8.8 was at the outermost side when  $0 < F_{V,Ed}/F_{V,Rd} < 0.7$ , while grade 10.9 was on the outermost side when  $0.7 < F_{V,Ed}/F_{V,Rd} < 1.0$ . In terms of GB-50017 formulas, the envelope of grade 10.9 was consistently at the outermost side, and the predicted ultimate resistance of grade 10.9 and 12.9 bolts was even lower than the design standard when  $N_v/N_v^b > 0.6$ . In terms of AISC-360 formulas, the evaluated ultimate strength of G10.9 was the highest

among the three grades when  $0.6 < V_f^*/V_f < 1.0$ , and when  $V_f^*/V_f > 0.8$ , the predictions for grade 8.8 and 12.9 high-strength bolts were less than the predicted values of specification. In terms of AS 4100 formulas, the curve of the design standard was enveloped by the predicted curve of grade 10.9, while the curves of grade 8.8 and 12.9 were intersected with a blue curve when  $V_f^*/V_f > 0.8$  and  $0.7$ , respectively.

### 3.2. Effects of bolt type

For bolts with a diameter 16 mm, zero-hole clearance, steel grade 10.9 but without preload force, the bolt ultimate resistance is predicted in terms of partially and fully threaded bolts. Table 4 and Fig. 7 compared the ultimate resistance of the two types of bolts under different loading conditions. The type of bolt is a key factor that

**Table 5**  
Simulated result of M20 and M24 bolt ultimate loading capacity.

Simulated grade 10.9 bolts			Tensile-shear displacement ratio ( $D_y/D_x$ )								
			UT	5	2	1.25	1	0.8	0.5	0.2	SH
$P_u$ (kN)	M20P	$P_y$	315.922	327.426	326.989	316.029	300.956	276.346	188.183	29.790	0
		$P_x$	0	62.368	96.177	103.305	120.774	151.245	189.823	233.244	241.361
		$P_u$	315.922	333.313	340.840	332.485	324.285	315.027	267.293	235.139	241.361
	M24P	$P_y$	455.281	470.461	483.447	468.342	456.719	423.991	295.929	30.642	0
		$P_x$	0	76.977	116.752	128.312	143.848	171.205	254.123	337.643	343.669
		$P_u$	455.281	476.717	497.346	485.601	478.836	457.253	390.068	339.031	343.669
	M20S	$P_y$	302.239	297.125	296.961	282.359	270.304	250.427	205.175	56.559	0
		$P_x$	0	11.278	31.838	52.157	69.106	88.508	129.651	176.443	193.982
		$P_u$	302.239	297.339	304.727	287.136	278.998	265.607	215.349	185.286	193.982
	M24S	$P_y$	444.683	443.590	431.386	412.108	392.133	359.900	269.003	61.380	0
		$P_x$	0	15.094	41.302	76.111	105.455	135.006	193.020	259.634	279.019
		$P_u$	444.683	443.847	433.359	419.077	406.065	384.389	331.088	266.791	279.019
$P_0$ (kN)	M20										
	M24									458.651	

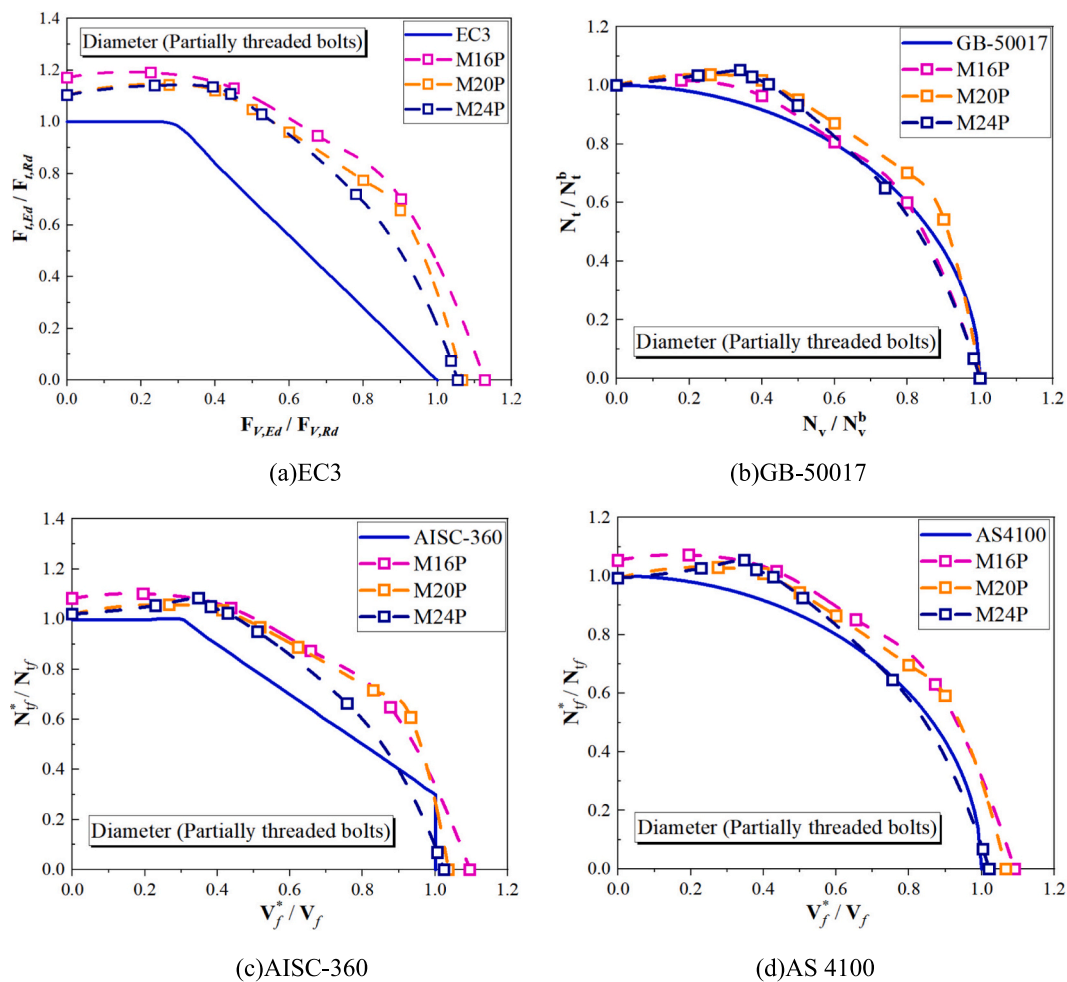


**Fig. 8.** Ultimate resistance comparisons with different diameter for partially threaded bolt.

influences the fracture behaviour of bolts. Compared to fully threaded bolts, partially threaded bolts exhibit higher load-carrying capacity. The absence of threads in the shear plane ensures that partially threaded bolts have higher shear strength. Additionally, the fracture deformations in both tension and shear directions are smaller for partially threaded bolts. This makes partially threaded bolts a safer choice for use in connection joints.

In terms of EC3 formulas, the envelopes of FE simulated resistance were on the outside of the suggested limits. The predicted ultimate

resistance from EC3 formulas have excessive safety redundancy in the tensile-shear coupling loading state when compared with simulation results. In terms of GB-50017 formulas, the envelopes of FE simulation results were on the outside of the suggested limits for the partially threaded bolts, but on the inside of the suggested limits for the fully threaded bolts. In terms of AISC-360 and AS 4100 formulas, the prediction of partially threaded bolts meet the requirements and falls inside of the suggested limits, but the assessment for fully threaded bolts was on unsafe side.

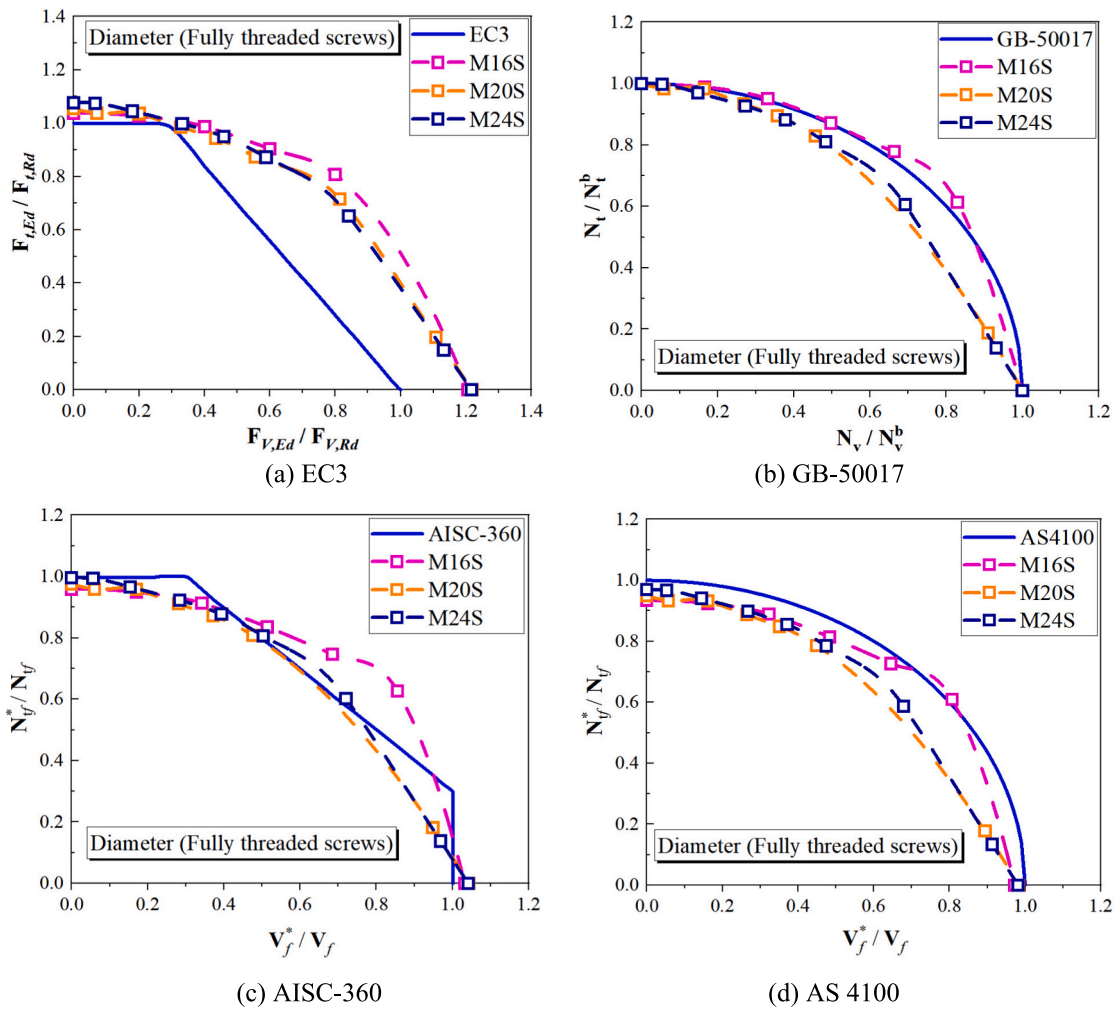


Fig. 9. Ultimate resistance comparisons with different diameter for fully threaded bolt.

### 3.3. Effects of bolt diameter

For bolts with zero-hole clearance, steel grade 10.9 but without preload force, the ultimate resistance of partially and fully threaded bolts is predicted in terms of diameters of 16 mm, 20 mm, and 24 mm respectively.

The ultimate resistance of M16 was listed in Table 4 in the previous sections. The ultimate resistance of M20 and M24 bolts was summarized in Table 5. Fig. 8 compared the ultimate resistance of partially threaded bolts with different diameters between theoretical values in four design codes and FE predicted results. When the bolts subject to combined tensile and shear loading, larger diameter bolts exhibit 2% ~ 4% higher nominal strength. As the same time, larger diameter bolts exhibited higher fracture deformation, 9.5% and 5.2% higher for partially and fully threaded bolts, respectively. In terms of EC3 formulas, the bolt resistance envelope with three different diameters are all on the outside of the suggested limits, but the utilization of bilinear lines may underestimate the resistance in the combined tensile-shear condition by 20%–30%. In terms of GB-50017 formulas, the bolts resistance from FE simulation was lower than the specification limits when  $N_v/N_v^b > 0.6$ . In terms of AISC-360 and AS 4100 formulas, the bolts resistance with diameters from FE simulation agreed well with specification limits.

Fig. 9 compared the ultimate resistance of fully threaded bolts with different diameters between theoretical values in four design codes and FE predicted results. In terms of EC3 formulas, the bolt resistance envelope with three different diameters are all on the outside of the suggested limits, especially the predicted values from formulas tends to be

conservative with increasing contribution of the shear force, that is  $0.4 < F_{V,Ed}/F_{V,Rd} < 1.0$ . However, in terms of GB-50017, AISC-360, and AS 4100 formulas, the suggested limits overpredicted the ultimate resistance for the bolts with all three diameters.

### 3.4. Effects of a bolt hole clearance

For partially and fully threaded bolts with a diameter 20 mm, steel grade 10.9 but without preload force, the bolt ultimate resistance is predicted in terms of 0 mm, 1 mm and 2 mm hole clearance. As shown in Fig. 10, the presence of the through-hole made partially threaded bolts slip when subjected to shear load, thus the strength of bolts with bolt hole clearance was the same as uniaxial tensile strength for shear ratios of 0–0.3. Bolt hole clearances had different degrees of damage for high-strength bolts, the larger gaps of bolts exhibited the lower ultimate resistance. Except for the uniaxial tension status, which did not be affected by gaps, the ultimate resistance was reduced in all other statuses under four specifications. Bolt hole clearance affects the maximum resistance of the partially threaded bolt, and the peak value decreases by about 2% for every 1 mm increase in gap. Fig. 11 shows a ultimate resistance comparison of fully threaded bolts, all four specifications are not safe for the evaluation of fully threaded bolts with hole clearance. The FE simulation results were lower than the formula predictions from EC3 when  $0 < F_{V,Ed}/F_{V,Rd} < 0.7$ , and were lower than the formula predictions of GB-50017, AISC-360, and AS 4100 in the whole range. For fully threaded bolts, the ultimate resistance drops sharply with the shear displacement increases, the presence of bolt hole clearance slows this

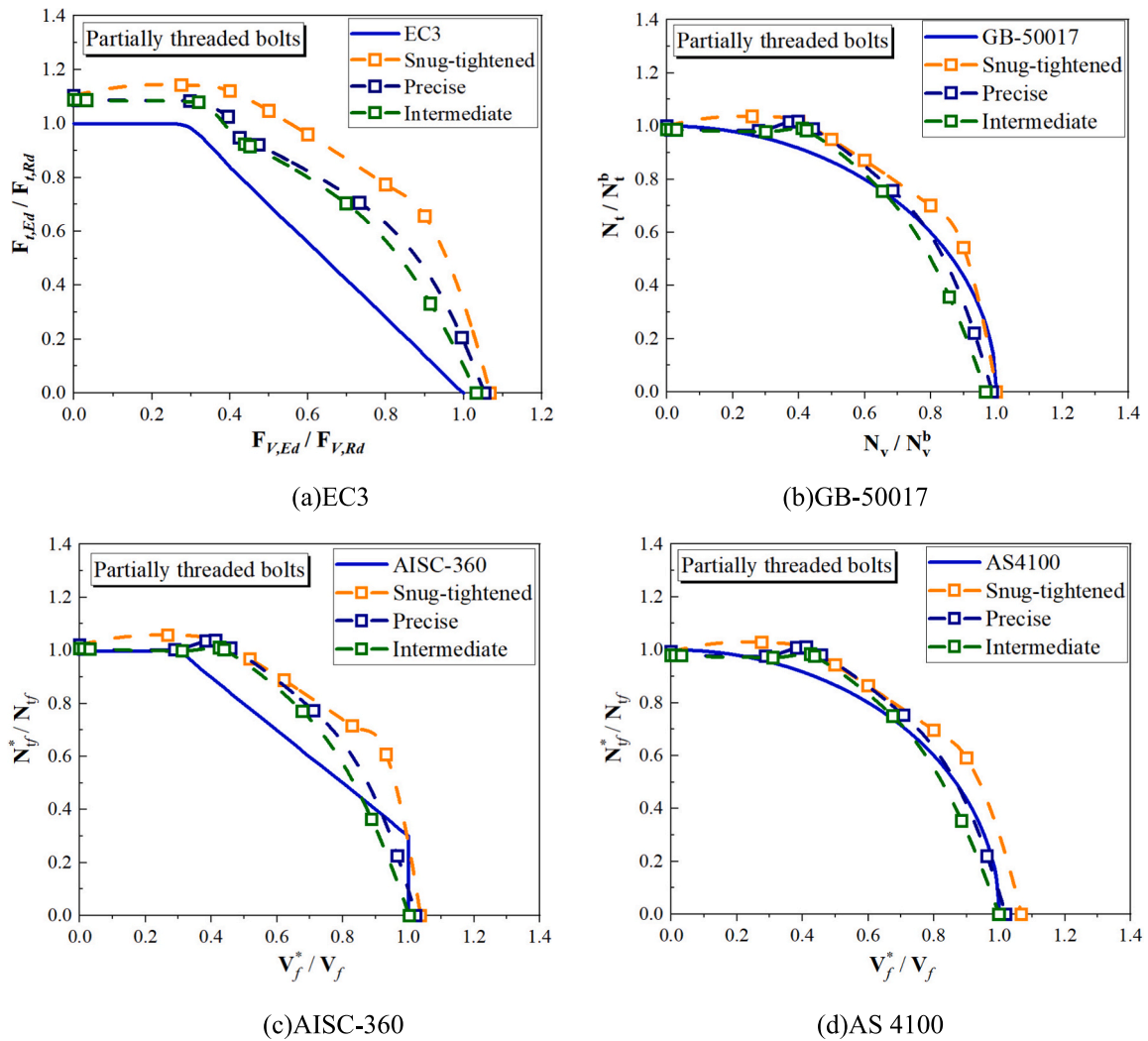


Fig. 10. Ultimate resistance comparisons with different hole clearance for partially threaded bolt.

trend but reduces the bearing capacity in the shear dominant state.

### 3.5. Effects of preload force

Controlling of the preload force is important to accomplish reliable connection, but too much preload force will lead to overload and fracture of the high-strength bolt [34]. The appropriate level of preload achieved during assembly is difficult to measure directly, hence various control methods such as torque-only, torque-turn/angle, bolt elongation, and torque-to-yield are generally used to control the preload level induced during installation [35]. The most common control of the preload force in construction site is by turning the nut angle. The partially threaded bolts with a diameter 20 mm, zero-hole clearance and steel grade 10.9 is used to investigate the preload force effects. The preload force appropriate is 170 kN achieved for a nut rotation of  $0.3\pi$  assuming the friction coefficient between threads of the nut and the bolt of 0.14, while the displacement in the tensile and shear directions is applied in the second step. A control group with no preload applied was used to compare the effect of preload level on the mechanical behaviour of the bolts. Table 6 compares the nominal stiffness of the bolts with different preload force level, the preload force level significantly increases the stiffness of the bolts, except for the pure shear (SH) state. The average stiffness of the bolt without preload was  $2.11 \times 10^6$  N/mm and was  $5.64 \times 10^6$  N/mm for pre-tensioned bolts, which increased the stiffness by  $3.53 \times 10^6$  N/mm.

Comparison of the ultimate resistance of the bolt with preload and without preload applied for four specifications is shown in Fig. 12. The results showed that the preload force level has negligible effects on the ultimate resistance when the tensile force is dominated (from 0 to 0.5 in X-axis) while a slightly decrease of ultimate resistance is observed when the shear force is dominated (from 0.5 to 1.0 in X-axis). For special states, normal bolts have a higher resistance in uniaxial tension, while bolts with preload have higher strength in pure shear. In summary, it can be explained that the application of preload will improve the stiffness of the bolt, making the fracture displacement of the bolt larger and ensuring the stability of the structure by absorbing more energy, although the preload does not affect the ultimate resistance of the high-strength bolt, it still has a great improvement on the safety of the structure.

## 4. Discussion of the result

According to the above, the current design standards are not satisfactory for the assessment of the ultimate resistance of high-strength bolts, they are either too conservative (EC3), too optimistic (GB-50017, AS 4100), or inaccurate for some load combinations (AISC-360). In addition, the type of bolt has a major effect on the accuracy of the prediction, and the evaluation formula needs to be divided into two categories depending on whether the shear surface passes through threaded part of the bolt or through the shank. In summary, it is

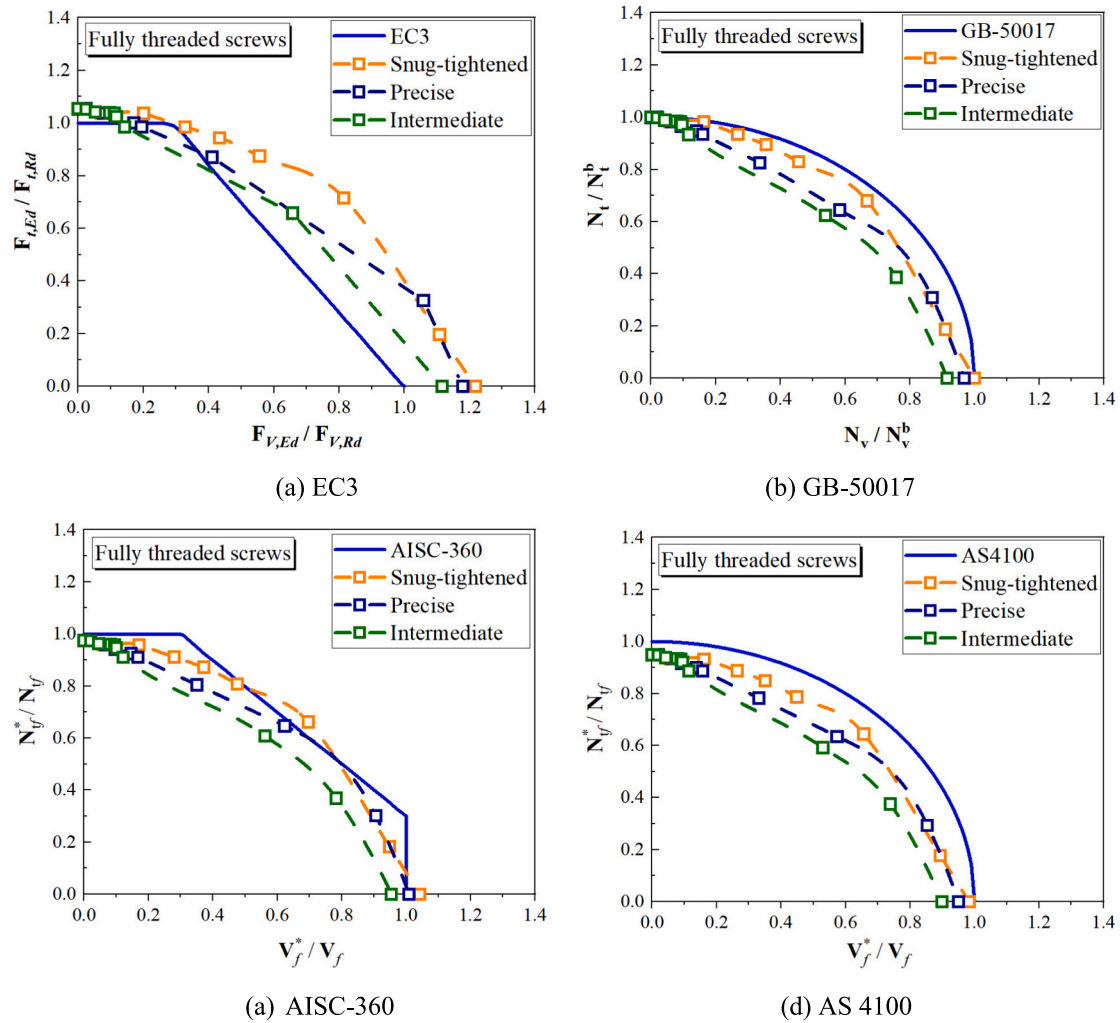


Fig. 11. Ultimate resistance comparisons with different hole clearance for fully threaded bolt.

Table 6

Comparisons of the nominal stiffness of bolts in various states.

Bolt	Nominal stiffness ( $\times 10^6$ N/mm)									
	UT	5	2	1.25	1	0.8	0.5	0.2	SH	
No pretension	2.10	2.12	2.15	2.10	2.07	2.13	2.08	2.16	2.12	
Pretension	5.42	5.95	5.98	5.59	5.72	5.55	5.59	5.32	2.11	

necessary to make some amendments to the international specifications to ensure better fit of the bolt resistance in different tensile and shear ratios compare to the existing tests and simulations.

4.1. Discuss Eurocode 3

Eurocode 3 was conservative compared to the prediction, which resulted in unnecessary design overstrength in the engineering practice. Therefore, the non-linear equation is recommended to a new prediction formula, as expressed in Eq. (1),  $\xi_v$ ,  $\xi_t$ , and  $m$  were used to ensure an accurate assessment. In addition, it was stipulated that  $\frac{F_{t,Ed}}{F_{t,Rd}} \leq 1$

$$\left(\frac{F_{V,Ed}}{\xi_v F_{V,Rd}}\right)^m + \left(\frac{F_{t,Ed}}{\xi_t F_{t,Rd}}\right)^m \leq 1.0 \tag{1}$$

As shown in Fig. 13, the orange line is the EC3 specification-modified formula with 95% assurance rates, and the blue was the original EC3 formula. With power coefficient  $m > 1$  to improve the design strength

and made better use of the bolt load resistance in a shear ratio between 0.4 and 1. For partially threaded bolts, the shear resistance is 0.4 ( $\xi_v = 0.94$ ), the tensile resistance is 1.40 ( $\xi_t = 1.40$ ), and the power coefficient is 1.30 ( $m = 1.30$ ). For fully threaded bolts, the conservative prediction under combined uniaxial tension-shear loading from current recommendations in European code EC3 can be improved by using  $\xi_v = 0.98$ ,  $\xi_t = 0.99$ , and  $m = 1.57$ .

4.2. Discuss GB-50017 and AS 4100

For the Chinese specification GB-50017 and the Australian specification AS 4100, we used the same expression, seen in Eq. (2). For the Chinese specification, the partially threaded bolts prediction was modified as  $\xi_v = 0.83$ ,  $\xi_t = 0.94$ , and  $m = 2.00$ .  $\xi_v = 0.79$ ,  $\xi_t = 0.94$ , and  $m = 1.66$  for fully threaded bolts, as expressed in Fig. 14, the modification factors for the Australian norms can be obtained in the same way that  $\xi_v = 0.89$ ,  $\xi_t = 0.92$ , and  $m = 2.00$  for partially threaded

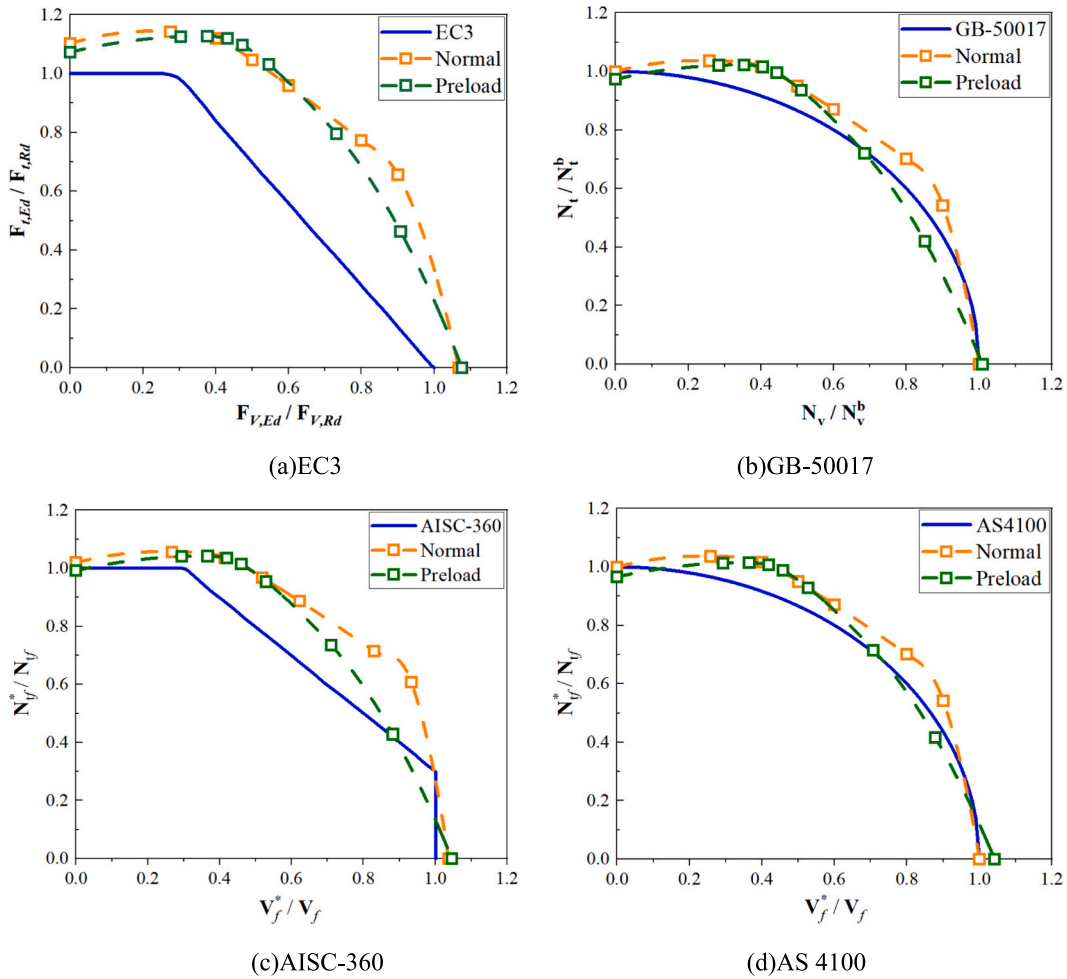


Fig. 12. Ultimate resistance comparisons with different preload force.

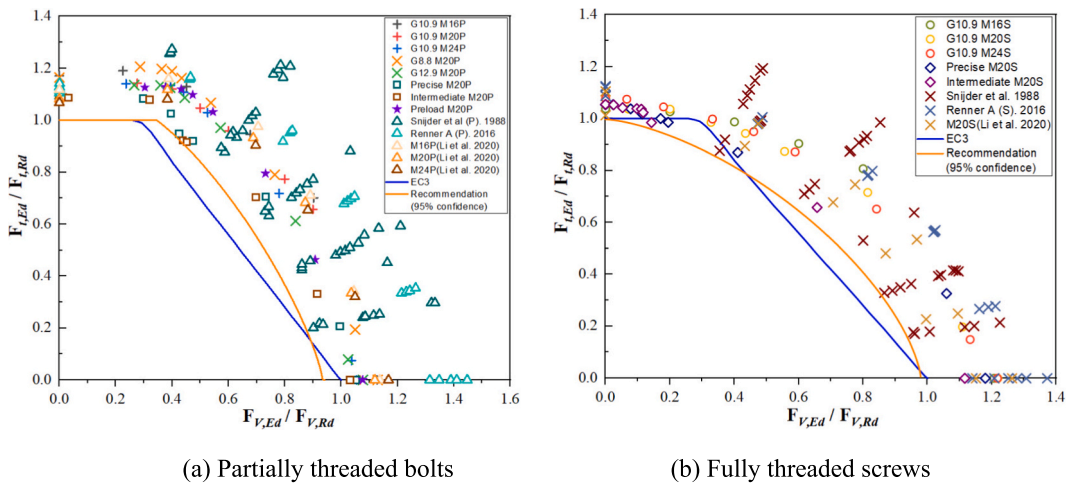


Fig. 13. Discussion of European code exponent.

bolts,  $\xi_v = 0.78$ ,  $\xi_t = 0.88$ , and  $m = 1.70$  for fully threaded bolts. The comparison of the modified formula at a 95% guarantee rate for AS 4100 and the original formula was shown in Fig. 15.

$$\left(\frac{N_v}{\xi_v N_v^b}\right)^m + \left(\frac{N_t}{\xi_t N_t^b}\right)^m \leq 1.0 \quad (2)$$

### 4.3. Discuss AISC-360

The AISC-360 specification for the combined tensile-shear status of the bolt's ultimate resistance prediction using a three-stage formula, the modification formula was shown in Eq. (3). Meanwhile, Eqs. (4) and (5) were proposed to ensure that the design strength was not aggressive in

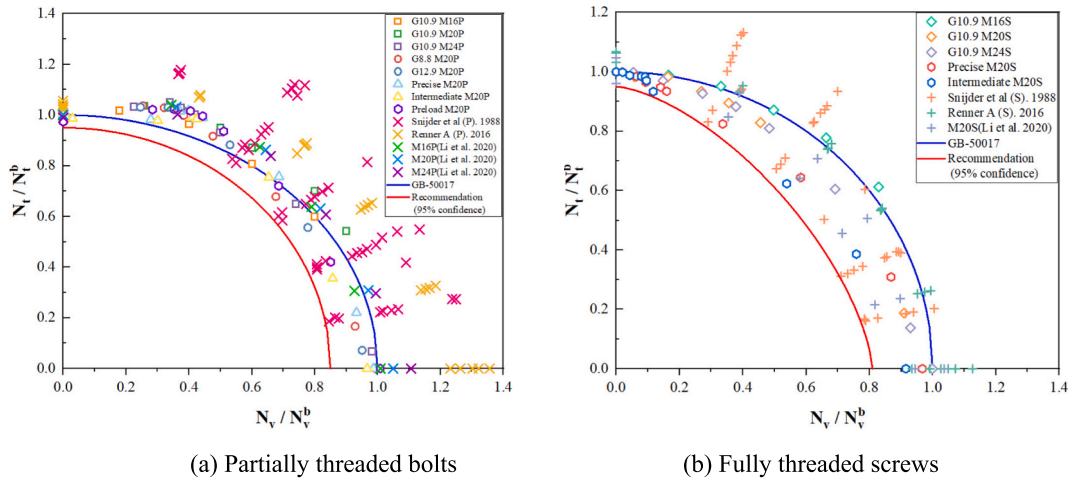


Fig. 14. Discussion of Chinese code exponent.

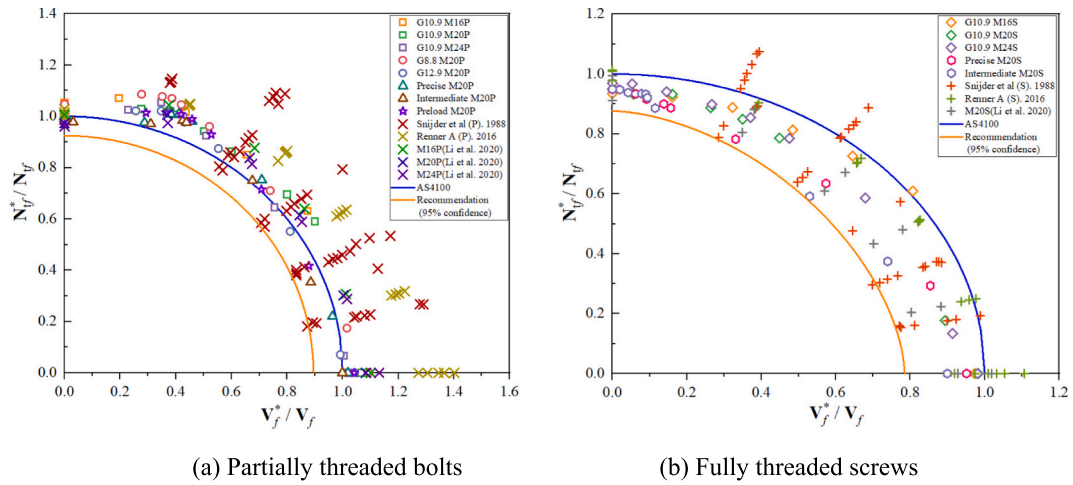


Fig. 15. Discussion of American code exponent.

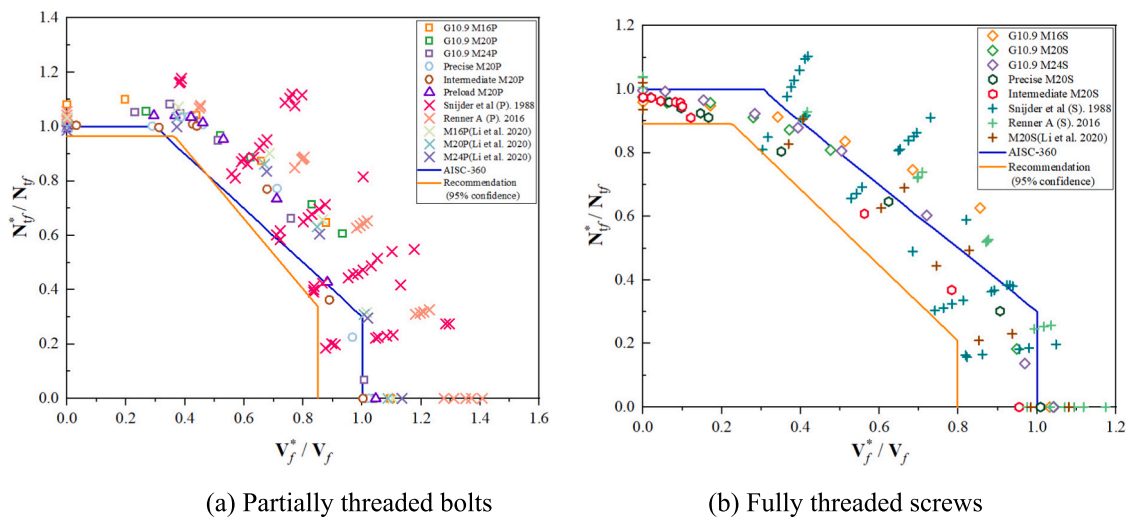


Fig. 16. Discussion of American code exponent.

uniaxial tension and pure shear states.

$$\frac{N_{fj}^*}{N_{fj}} + k \frac{V_f^*}{V_f} < C \quad (3)$$

$$\frac{V_f^*}{V_f} \leq \gamma_v \quad (4)$$

$$\frac{N_{fj}^*}{N_{fj}} \leq \gamma_t \quad (5)$$

Partially threaded bolts had high tensile and shear strength, the  $\gamma_v$  and  $\gamma_t$  were calibrated as 0.85 and 0.96. The loading factor for shear resistance  $k$  and linear expansion factor  $C$  can be obtained as 1.29 and 1.43, respectively. For fully threaded bolts, the uniaxial tensile and shear strength were lower than partially threaded bolts,  $\gamma_v$  was obtained as 0.8,  $\gamma_t$  is 0.89, and  $k = 1.19$ ,  $C = 1.16$ . Fig. 16 illustrated the effectiveness of the AISC-360 modified formula for the prediction of high-strength bolts.

## 5. Conclusion

Simulations on high-strength bolts with various factors were conducted at combined tension-shear loading. Each type of bolt was subjected from uniaxial tension to pure shear to obtain the ultimate resistance and fracture deformation, and the effects of grade, type, diameter, bolt hole clearance, and pre-loading were investigated. The simulated results were further compared with the current international standards. Corresponding design recommendations and modified design strength equations were proposed. The following conclusions can be drawn:

1. The assessment of the three grades of bolts in EC3 is biased towards safety, while GB-50017, AISC-360, and AS 4100 are aggressive for G8.8 in the shear-dominated state, and the same assessment equations are not applicable for G12.9.
2. A comparison with the code shows that the simulated shear load is 6% higher for partially threaded bolts and 22% higher for fully threaded bolts than the theoretical value of EC3. AISC-360, GB-50017, and AS 4100 have accurate predictions for partially threaded bolts but are overestimated for fully threaded bolts in the full process.

## Appendix A

### A.1. Stress-strain relationship

The material at the necking region changes from a uniaxial stress state to a triaxial stress state when necking occurs in high-strength steel tensile specimens, the post-necking true stress-strain curve cannot be obtained directly from the engineering stress-strain relationship. A suitable degradation function is required to express the true stress-strain curve of the material after necking, such as the weighting function shown in Eq. (6), which targets the measured engineering stress-strain and calibrates the weight constant  $W$  to meet the accuracy requirements of the engineering stress-strain relationship calculated in the finite element model.

$$\bar{\sigma}^{neck} = \bar{\sigma}_u \left[ W(1 + \bar{\epsilon}^p - \bar{\epsilon}_u^p) + (1 - W) \left( \frac{(\bar{\epsilon}^p)^{\bar{\epsilon}_u^p}}{(\bar{\epsilon}_u^p)^{\bar{\epsilon}_u^p}} \right) \right] \quad (6)$$

Furthermore, the damage scalar  $d$  is varied in the FE model to obtain a good fit to the target engineering stress-strain curve, which continues as material damage progresses as expressed in Eqs. (7–8).

$$\bar{\sigma} = (1 - d)\bar{\sigma}^{neck} \quad (7)$$

$$d = \begin{cases} 0 & \bar{\epsilon}^p < \bar{\epsilon}_{d-i}^p \\ 1 - \exp[-B(\bar{\epsilon}^p - \bar{\epsilon}_{d-i}^p)] & \bar{\epsilon}^p \geq \bar{\epsilon}_{d-i}^p \end{cases} \quad (8)$$

Reference [27] provides comprehensive instructions for calibrating the parameters for the post-necking true stress-strain curve

3. For Eurocode 3, the modification factors  $\xi_t$ ,  $\xi_v$ , and  $m$  are 1.40, 0.94, and 1.30 for the partially threaded bolt and 0.99, 0.98, 1.57 for the fully threaded bolt. For GB-50017, the better fits occurred for partially threaded bolt when  $\xi_v = 0.83$ ,  $\xi_t = 0.94$ , and  $m = 2.00$ .  $\xi_v = 0.79$ ,  $\xi_t = 0.94$ , and  $m = 1.66$  for fully threaded bolt. For AS 4100, the predictions are modified as  $\xi_v = 0.89$ ,  $\xi_t = 0.92$ , and  $m = 2.00$  for partially threaded bolts,  $\xi_v = 0.78$ ,  $\xi_t = 0.88$ , and  $m = 1.70$  for fully threaded bolts. For AISC-360, the prediction equation of the same form as the existing specification is proposed, and the adjustment parameters of partially threaded bolts are:  $\gamma_v = 0.85$ ,  $\gamma_t = 0.96$ ,  $k = 1.29$ , and  $C = 1.43$ . For fully threaded bolts, the four factors are 0.80, 0.89, 1.19 and 1.16 respectively.

## CRedit authorship contribution statement

**Haohui Xin:** Conceptualization, Methodology, Validation, Writing – review & editing. **Gao Liu:** Writing – review & editing, Methodology, Validation. **Youyou Zhang:** Writing – review & editing, Methodology, Validation. **Jie Li:** Formal analysis, Writing – original draft. **Milan Veljkovic:** Writing – review & editing, Supervision.

## Declaration of competing interest

The authors declare that they have no known competing financial interests or personal relationships that could have appeared to influence the work reported in this paper.

## Data availability

Data will be made available on request.

## Acknowledgement

This paper is supported by the Systematic Project of Guangxi Key Laboratory of Disaster Prevention and Engineering Safety (Grant Number: 2022ZDK009), Qin Chuangyuan's "Scientist + Engineer" team construction project (2024QCY-KXJ-159), Science and Technology Plan of Xi'an City's "Scientist + Engineer" team construction project (2023JH-DWJS-0025).

## A.2. Ductile fracture parameter identification

The fracture of the bolt is realized by calibrating the fracture locus and defining the damage initiation criterion in ABAQUS. The fracture locus is given as a function of stress triaxiality and Lode parameter [36] as below Eq. (10).

$$\bar{\epsilon}_{pl,f}^p = C_3 \left( \frac{\sqrt{\bar{L}^2 + 3}}{2} \right)^{C_1} \left[ \frac{1}{1+C} \left( \bar{\eta} + \frac{3-\bar{L}}{3\sqrt{\bar{L}^2 + 3}} + C \right) \right]^{-C_2} \quad (10)$$

The values of  $C_1$ ,  $C_2$ , and  $C_3$  are obtained by computational homogenization at the level of unit cell based on the mesoscale critical equivalent plastic strain (MCEPS) method. Reference [28, 29] provides comprehensive instructions for calibrating the parameters for the above fracture locus.

## Appendix B

The ultimate resistance formulas of high-strength bolts were reported in different steel structures design specifications, including GB-50017 [5], EC3 [6], AISC-360 [7], and AS 4100 [8]. The details of the ultimate capacity formulas will be explained in the below section.

### B.1. European standard (Eurocode 3)

In the Eurocode 3 [6] design specification, the ultimate design resistance for the bolt subjected to different loading patterns is expressed as:

$$F_{t,Rd} = \frac{k_2 f_u^b A_s}{\gamma_{M2}} \quad (11)$$

$$F_{v,Rd} = \frac{\alpha_v f_u^b A}{\gamma_{M2}} \quad (12)$$

$$\frac{F_{V,Ed}}{F_{V,Rd}} + \frac{F_{t,Ed}}{1.4 F_{t,Rd}} \leq 1.0 \quad (13)$$

To compare the ultimate resistance between finite element simulation and formulas in the EC3 design specification, the  $\gamma_{M2}$  is assumed as 1.0. It means that the characteristic value, according to the terminology of EC3, is used for comparison with FE predictions. The design value (the name will remain in the text for the sake of simplicity) of combined tensile and shear loading is in the form of a linear relationship, and a “stretch” factor of 1.4 is given to increase the slope of the line. The ratio  $\frac{F_{t,Ed}}{F_{t,Rd}} \leq 1$  is used to control the pure tensile resistance.

### B.2. Chinese standard (GB-50017)

In the GB-50017 [5] design standard, the design equation of the ultimate capacity of bolts in pure shear or tension loading, as well as combined shear and tension loading is expressed below:

$$N_t^b = f_t^b A_s \quad (14)$$

$$N_v^b = f_v^b A \quad (15)$$

$$\sqrt{\left( \frac{N_v}{N_v^b} \right)^2 + \left( \frac{N_t}{N_t^b} \right)^2} \leq 1.0 \quad (16)$$

Noted that GB-50017 does not discriminate the failure mode whether the shear plane passes through the threads during shear resistance evaluation.

### B.3. American standard (AISC-360)

The load and resistance factor design (LRFD) method are employed in the American standard (AISC-360 [7]) for the resistance evaluation. The related evaluation formulas are as follows:

$$R_n = F_{nt}' A_b \quad (17)$$

$$R_n = F_{nv}' A_b \quad (18)$$

$$F_{nt}' = 1.3 F_{nt} - \frac{F_{nt}}{\phi F_{nv}} f_{rv} \leq F_{nt} \quad (19)$$

$$F_{nv}' = 1.3 F_{nv} - \frac{F_{nv}}{\phi F_{nt}} f_{rt} \leq F_{nv} \quad (20)$$

AISC-360 grouped the high-strength bolts according to material strength in Table 7.

**Table 7**  
Strength class of high-strength bolts under AISC-360 [7].

	Nominal Tensile Strength (MPa)	Nominal Shear Strength in bearing-type connections (MPa)	
		Threads to the shear plane	
Group A	620	excluded	372
		included	469
Group B	780	excluded	469
		included	579
Group C	1040	excluded	620
		included	779

#### B.4. Australia standard (AS 4100)

The ultimate resistance expressions of bolts in AS 4100 [8] are as below:

$$N_{tf}^* \leq \Phi N_{tf} \quad (21)$$

$$N_{tf} = A_s f_{tf} \quad (22)$$

$$V_f^* \leq \Phi V_f \quad (23)$$

$$V_f = 0.62 f_{tf} k_r (n_n A_c + n_x A_0) \quad (24)$$

$$\left( \frac{V_f^*}{\Phi V_f} \right)^2 + \left( \frac{N_{tf}^*}{\Phi N_{tf}} \right)^2 \leq 1.0 \quad (25)$$

#### References

- B. Yang, K.H. Tan, Experimental tests of different types of bolted steel beam-column joints under a central-column-removal scenario, *Eng. Struct.* 54 (2013) 112–130.
- B. Yang, K.H. Tan, Numerical analyses of steel beam-column joints subjected to catenary action under in-plane loading, *J. Constr. Steel Res.* 70 (2009) 1–11.
- IStructE, Safety in Tall Buildings and Other Buildings with Large Occupancy, Institution of Structural Engineers, London, UK, 2002.
- B. Meng, Y. Xiong, W. Zhong, S. Duan, H. Li, Progressive collapse behaviour of composite substructure with large rectangular beam-web openings, *Eng. Struct.* 295 (2023) 116861.
- GB 50017–2017, Standard for Design of Steel Structures, Beijing, 2018.
- Eurocode 3, Design of Steel Structures, Part 1.8, Design of joints, BS EN 1993-1-8 2005, 2005, UK, London.
- ANSI/AISC-360-16, Specification for Structural Steel Buildings, AISC, Chicago, 2016.
- A.S. Standards Australia, 4100–1998: Steel, Structures (2016) 99–101SAI, 1999.
- L. Bull, E.J. Palmiere, R.P. Thackray, I.W. Burgess, B. Davison, Tensile behaviour of galvanised grade 8.8 bolt assemblies in fire, *J. Struct. Fire Eng.* 6 (3) (2024) 197–212.
- F. Hanus, G. Zilli, J.M. Franssen, Behaviour of grade 8.8 bolts under natural fire conditions-tests and model, *J. Constr. Steel Res.* 67 (2011) 1292–1298.
- B.R. Kirby, The behaviour of high-strength grade 8.8 bolts in fire, *J. Constr. Steel Res.* 33 (1995) 3–38.
- G.H. Sterling, J.W. Fisher, "Tests of A490 Bolts." Fritz Engineering Lab. Report, No. 288.15, Lehigh University. Standards Australia, AS 4100–1998:Steel Structures 2016, 1964.
- R.S. Nair, P.C. Birkemoe, W.H. Munse, High strength bolts subject to tension and prying, *J. Struct. Div. ASCE* 100 (2) (1974) 351–372.
- J.J. Amrine, J.A. Swanson, Effects of variable pretension on the behavior of bolted connections with prying, in: *Engineering Journal*, American Institute of Steel Construction, 3rd Quarter, 2004, 2004.
- E. Chesson, N.L. Faustino, W.H. Munse, High-strength bolts subjected to tension and shear, *J. Struct. Div. ASCE* 91 (5) (1965) 155–180.
- A.K. Kawohl, J. Lange, Tests on 10.9 bolts under combined tension and shear, *Acta Polytechn.* 56 (2) (2016) 112–117.
- M. D'Aniello, D. Cassiano, R. Landolfo, Monotonic and cyclic inelastic tensile response of European preloadable gr10.9 bolt assemblies, *J. Constr. Steel Res.* 124 (2016) 77–90.
- H. Ketabdari, A. Saedi Daryan, N. Hassani, Predicting post-fire mechanical properties of grade 8.8 and 10.9 steel bolts, *J. Constr. Steel Res.* (2019) 162.
- D. Li, B. Uy, J. Wang, Y. Song, Behaviour and design of high-strength grade 12.9 bolts under combined tension and shear, *J. Constr. Steel Res.* 174 (2020) 106305.
- I.S.O. 898–1, ISO Mechanical properties of fasteners made of carbon steel and alloy steel, in: Part 1: Bolts, Screws and Studs with Specified Property Classes - Coarse Thread and Fine Pitch Thread, 2009.
- A.S.T.M. Standard F606, Standard Test Methods for Determining the Mechanical Properties of Externally and Internally Threaded Fasteners, Washers, Direct Tension Indicators, and Rivets, ASTM International, West Conshohocken, PA, 2003, p. 2016.
- A.A. Hedayat, E.A. Afzadi, A. Iranpour, Prediction of the bolt fracture in shear using finite element method, *Structures* 12 (2017) 188–210.
- M. Seif, et al., Finite element modeling of structural steel component failure at elevated 631 temperatures, *Structures* 6 (2016) 134–145.
- M. Hadjoannou, E.B. Williamson, M.D. Engelhardt, Collapse simulations of steel-concrete composite floors under column loss scenarios, *J. Struct. Eng.* 146 (12) (2020).
- H. Xin, J. Li, M. Veljkovic, et al., Evaluating the Strength of Grade 10.9 Bolts Subject to Multiaxial Loading Using the Micromechanical Failure Index: MCEPS, *Steel Construction-Design and Research*, February, 2022.
- B. Reeder, P. Grimmer, J. Emery, Cohesive zone models for reduced-order 578 fastener failure, in: *AIAA SciTech Forum*, 2019, San Diego, CA.
- H. Xin, M. Veljkovic, Evaluation of high strength steels fracture based on uniaxial stress-strain curves, *Eng. Fail. Anal.* 120 (2021) 105025.
- H. Xin, M. Veljkovic, J.A. Correia, F. Berto, Ductile fracture locus identification using mesoscale critical equivalent plastic strain, *Fatigue Fract. Eng. Mater. Struct.* 44 (5) (2021) 1292–1304.
- H. Xin, J.A.F.O. Correia, M. Veljkovic, F. Berto, Fracture parameters calibration and validation for the high strength steel based on the mesoscale failure index, *Theor. Appl. Fract. Mech.* 112 (2021) 102929.
- D. Li, B. Uy, J. Wang, Y. Song, Behaviour and design of grade 10.9 high-strength bolts under combined actions, *steel, Compos. Struct.* 35 (3) (2020) 327–341.
- J. Li, H. Xin, J.A.F.O. Correia, et al., Mesh size effects on fracture locus of high strength bolts: a mesoscale critical equivalent plastic strain (MCEPS) approach, *Eng. Fail. Anal.* 138 (2022) 106385.
- ISO 262:2:1998, ISO General Purpose Metric Screw Threads — Selected Sizes for Screws, Bolts and Nuts, 1998.
- EN 14399–3:2015, High-strength Structural Bolting Assemblies for Preloading - Part 3: System HR - Hexagon Bolt and Nut Assemblies, 2015.
- M. Cabrera, W. Tizani, J. Ninic, F. Wang, Experimental and numerical analysis of preload in extended hollo-bolt blind bolts, *J. Constr. Steel Res.* 186 (2021) 106885.
- T. Sakai, *Bolted Joint Engineering Fundamentals and Applications*. Beuth, 2008 (Accessed June 10, 2022).
- Y. Lou, J.W. Yoon, H. Huh, Modeling of shear ductile fracture considering a changeable cut-off value for stress triaxiality, *Int. J. Plast.* 54 (2014) 56–80.